Long-distance quantum state transfer via disorder-robust magnons

W. V. P. de Lima

Instituto de Física, Universidade Federal de Alagoas, 57072-970 Maceió, Alagoas, Brazil

F. A. B. F. de Moura

Instituto de Física, Universidade Federal de Alagoas, 57072-970 Maceió, Alagoas, Brazil

D. B. da Fonseca

Departamento de Física, Universidade Federal Rural de Pernambuco, 52171-900 Recife, Pernambuco 52171-900, Brazil

F. Moraes

Departamento de Física, Universidade Federal Rural de Pernambuco, 52171-900 Recife, Pernambuco 52171-900, Brazil

A. L. R. Barbosa

Departamento de Física, Universidade Federal Rural de Pernambuco, 52171-900 Recife, Pernambuco 52171-900, Brazil

G. M. A. Almeida

Instituto de Física, Universidade Federal de Alagoas, 57072-970 Maceió, Alagoas, Brazil

E-mail: gmaalmeida@fis.ufal.br

Abstract. Magnon-based quantum state transfer of a qubit is investigated in a one-dimensional Heisenberg model featuring uncorrelated disorder. In the weak coupling regime with respect do the boundaries of the channel, the presence of an anomalous magnon mode with diverging localization length is harnessed to promote high-fidelity state transfer despite the degree of exchange coupling disorder. Under the additional influence of diagonal disorder due to the external magnetic field, we explore ways to optimize the transfer fidelity by navigating through the disordered landscape so as to identify extended states within the channel. Our results are relevant to the design of magnon-based devices for information processing and communication amid the fast-paced progress in the field of magnonics.

1. Introduction

The success of data manipulation and storage in magnetic materials in the last few decades has prompted the field of spintronics to develop into several branches [1, 2]. One of these is magnonics, which envisions fundamental collective spin excitations (or magnons) as information carriers in the micro- and nanoscale [3]. Spin waves do not involve actual motion of particles in space and so they beat standard electronics with respect to energy dissipation due to the lack of Joule heat. Another advantage is the relative easiness to drive a spin system into nonlinear regimes, thereby providing with novel resources such as multi-magnon enhanced interaction [4], magnetic solitons [5] and Bose-Einstein condensates [6, 7].

The coherent nature of spin dynamics can also be harnessed for the realization of logic gates in magnon-based computation, light-matter interfaces, and more [3, 8, 9]. Although spintronics exists in its own realm, we have witnessed its integration with quantum information processing over the years. Indeed, a whole field known as *quantum magnonics* [10] has been surging with the goal of designing hybrid platforms that couple magnons to other quantum systems including phonons, optical photons, and superconducting qubits [11].

It is natural to think of spin systems as solid state models for quantum computation where, e.g., spin$-1/2$ particles can act as qubits with their coupling mediated by spin-spin exchange interactions. Indeed, with the goal of transmitting qubit coherent states and distributing entanglement, spin chains are promising platforms for quantum networks [12, 13, 14, 15, 16, 17]. Overall, achieving tailored coherent magnon dynamics is paramount when interfacing spin chains with other quantum systems [11, 18, 19, 20, 21].

A basic requirement in any spin-based quantum device is the capability of transmitting a spin excitation between distant sites with high fidelity, to which various Hamiltonian engineering schemes have been proposed, especially on the isotropic XY model [22, 23, 24, 25, 26, 27, 28, 25, 29, 30, 31, 32, 33]. In reality, the transmission performance will depend on various factors including decoherence rate, state initialization and measurement, control noise, physical platform, and manufacturing imperfections. The latter leads to disorder, potentially resulting in an incoherent (or diffusive) spin wave propagation [34]. While disorder is generally detrimental to the state transfer quality [30, 35, 36, 37, 38, 39], spin chains with modified boundary couplings [40, 41] are particularly robust against it [38], even more so when the disorder is correlated [42, 43, 44, 45, 46]. In these cases, the correlation imprinted in the disorder distribution promote the emergence of extended states among strongly-localized states, what facilitates quantum communication mediated by long channels.

In this work, however, we investigate the coherent state transfer of a qubit encoded in a Heisenberg linear chain featuring diagonal and off-diagonal *uncorrelated* disorder (see scheme in Fig. 1). The absence of correlations in the disorder renders the system more susceptible to Anderson localization effects [47]. Yet, we demonstrate that leveraging correlations intrinsic to the Heisenberg interaction allows for end-to-end

quantum communication with high-fidelity. This is done upon a judicious tuning of the external magnetic fields acting on both outer spins, besides weak end couplings. Two distinct scenarios are addressed. In the first case, we explore a resonant state transfer mediated by an anomalous uniform magnon mode that is fully resistant to the off-diagonal (exchange coupling) disorder. A scaling law for the fidelity $F = 1 - O(g^2N^3)$ is derived with respect to the channel size N and boundary couplings g. In the second scenario, we discuss the conditions for off-resonant high-fidelity state transfer based on the availability of extended states within the channel. We will see that the competition between both types of disorder enforces an optimal local energy for the communicating spins, which is in the vicinity of the energy that corresponds the anomalous magnon mode.

2. Methods

Consider a chain of $N+2$ spin$-1/2$ particles interacting via the Heisenberg Hamiltonian $\mathcal{H} = \mathcal{H}_{\rm end} + \mathcal{H}_{\rm ch}$, where

$$\mathcal{H}_{\rm end} = -2g(\vec{S}_1 \cdot \vec{S}_2 + \vec{S}_{N+1} \cdot \vec{S}_{N+2}) - \vec{h}_1 \cdot \vec{S}_1 - \vec{h}_{N+2} \cdot \vec{S}_{N+2}, \tag{1}$$

$$\mathcal{H}_{\rm ch} = -\sum_{n=2}^{N} J_n \vec{S}_n \cdot \vec{S}_{n+1} - \sum_{n=2}^{N+1} \vec{h}_n \cdot \vec{S}_n. \tag{2}$$

Here, the $\vec{S}_n$ is the spin operator at site n, $J_n = J(1+u_n)$ is the exchange coupling strength, and $\vec{h}_n$ is the local magnetic field. The first and last spins (labeled by indexes 1 and $N+2$, respectively) are coupled to the channel (bulk) via the parameter g, which we set $g \ll J$. Throughout this paper the energy is always expressed in units of $J \equiv 1$.

The channel, modeled by $\mathcal{H}_{\rm ch}$, is assumed to be disordered. We consider that u_n and h_n are independent random variables uniformly distributed in $[-W_J/2, W_J/2]$ and $[-W_h/2, W_h/2]$, respectively, restricted to $W_J < 1$ and $W_h < 1$. The magnetic fields h_1 and h_{N+2} are set such that their corresponding diagonal elements read $\mathcal{H}_{1,1} = \mathcal{H}_{N+2,N+2} = h_0$. With this parameter we can suitably tune the end spin states with magnon modes that maximize the transfer performance [42, 43, 44].

The qubit to be sent through the channel is prepared as $|\phi_1\rangle = \alpha|\downarrow_1\rangle + \beta|\uparrow_1\rangle$ on top of the ferromagnetic ground state $|\Downarrow\rangle$ – namely, all the other spins down or, in the single particle language, the vacuum state – so that the input state reads $|\Psi_{\rm in}\rangle = |\phi_1\rangle|\downarrow_2\rangle\cdots|\downarrow_{N+2}\rangle$. The Hamiltonian $\mathcal{H}$ preserves the net magnetization of the system, rendering the spin wave to propagate in the single-excitation sector only. Therefore, this symmetry ensures there is no interaction with higher magnon states. Note that when the external magnetic field W_h is finite but weak, the ground state undergoes small perturbations around a preferred direction of alignment. While the spins may be slightly misaligned due to the disorder, the direction of the average magnetization remains approximately fixed, allowing us to linearize the fluctuations around this direction. Hereafter, we denote a state representing a spin flipped at site n

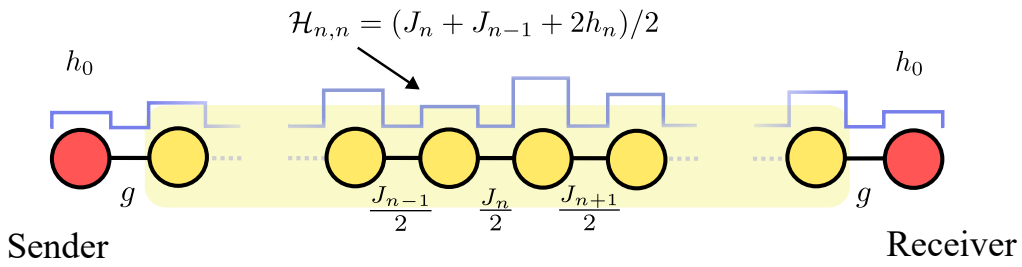

Figure 1. Sketch of the quantum-state transfer scheme involving the one-magnon states. The sender and receiver have access to the first and last nodes, respectively. Both are weakly coupled to the channel (bulk) with strength g. All the edge rates are shown up to a minus sign. The effective local energies $\mathcal{H}_{n,n}$ combine both exchange couplings J_n and magnetic fields h_n, which are random variables, with exception of h_1 and h_{N+2}. These are taken as tunable parameters that provide $\mathcal{H}_{1,1} = \mathcal{H}_{N+2,N+2} = h_0$.

as $|n\rangle = |\downarrow_1\rangle|\downarrow_2\rangle\cdots|\uparrow_n\rangle\cdots|\downarrow_{N+2}\rangle$. The input is recast as $|\Psi_{\rm in}\rangle = \alpha|\Downarrow\rangle + \beta|1\rangle$. We mention that this kind of spin chain quench can be realized in photonic platforms [48].

The goal of the state transfer protocol is to maximize the conversion of the state $|1\rangle$ to $|N+2\rangle$ by means of the Hamiltonian time evolution while preserving the phase relationship of the encoded qubit. The protocol performance is measured by the transfer fidelity averaged over the input's Bloch sphere, parameterized by α and β, [22]:

$$F(t) = \frac{1}{2} + \frac{|a_{N+2}(t)|}{3}\cos\xi + \frac{|a_{N+2}(t)|^2}{6}, \tag{3}$$

where $a_n(t) = \langle n|\mathcal{U}(t)|1\rangle$ is the transition amplitude between sites 1 and n, and $\mathcal{U}(t) = e^{-i\mathcal{H}t}$ is the quantum time-evolution operator (time is expressed in units of J^{-1}). The output phase can be offset, $\cos\xi \equiv 1$, by adjusting the external magnetic field or applying a local rotation to the last spin at the end of the protocol. The average fidelity is thus bounded between 1/2 and 1.

The transition amplitudes $a_n(t)$ obey the Schrödinger equation

$$\left(\frac{J_n}{2} + \frac{J_{n-1}}{2} + h_n\right) a_n - \frac{J_n}{2}a_{n+1} - \frac{J_{n-1}}{2}a_{n-1} = i\frac{da_n}{dt}. \tag{4}$$

The single-particle graph structure involving states $|1\rangle$ through $|N+2\rangle$ is depicted in Fig. 1. Note that our system be mapped onto a tight-binding model or, more specifically, the isotropic XY model (often addressed in the context of quantum state transfer [22]) having those coupling parameters.

Alternatively, we can expand

$$a_n(t) = \sum_{k=1}^{N+2}\langle n|\lambda_k\rangle\langle\lambda_k|1\rangle e^{-i\lambda_k t}, \tag{5}$$

where the eigenvalues λ_k and eigenvectors $|\lambda_k\rangle$ are obtained here via exact numerical diagonalization of $\mathcal{H}$. All the quantities of interest presented below are averaged over many independent realizations of the disordered Hamiltonian.

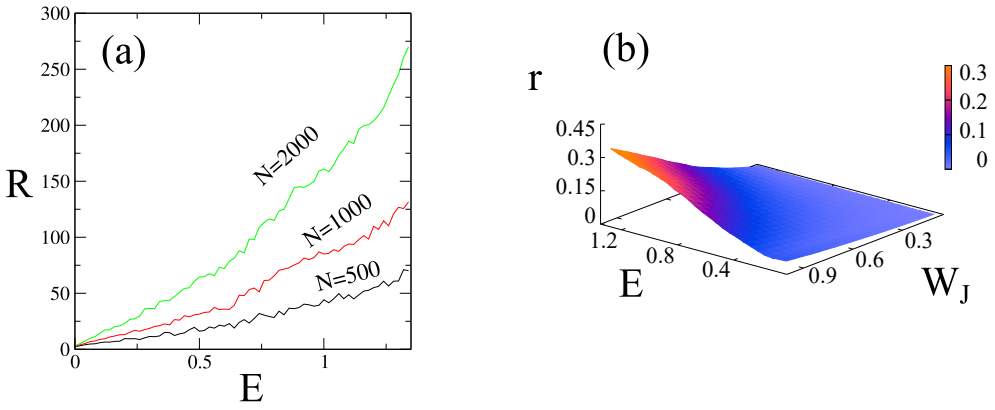

Figure 2. (a) Localization measure $R = rN$ versus E, with r given by Eq. (6). Channel parameters are for $W_J = 0.5$, $W_h = 0$, and various system sizes are considered as indicated in the figure. (b) Function r versus E and W_J considering $N = 500$. Displayed results are averaged over 5000 independent realizations of disorder.

3. Results

In the following we provide a brief overview of the channel's localization properties. We then proceed to address two distinct quantum communication schemes that function under the condition $g \ll 1$. The first one relies on a resonance between the outer spins and the anomalous extended magnon mode. The second scheme strategically goes off-resonant so as to bypass the effects of the disordered magnetic field.

3.1. Localization properties

Before diving into the state transfer protocol itself, let us explore some spectral properties of the channel described by $\mathcal{H}_{\rm ch}$ [see Eq. (2)]. The purpose here is to search for extended magnon states within the energy band, as their presence will impact our adjustment of the local magnetic field h_0 later. For now, we define the external magnetic field homogeneous (by setting $W_h \equiv 0$ for convenience).

To characterize localized states, we employ the quantity

$$r_k = \max\{|v_{k,n}|^2\} - \min\{|v_{k,n}|^2\}, \tag{6}$$

where $v_{k,n} = \langle n|\psi_k\rangle$ is the channel wavefunction at n ($n = 2, \ldots, N+1$) with respect to the energy E_k. Since many disorder realizations are considered, in effect we calculate $r(E) = \sum_{|E_k - E| < \delta E}(r_k/N_k)$, where N_k is the number of eigenvalues within $[E - \delta E/2, E + \delta E/2]$. We fix the energy bin to $\delta E \approx 0.05$. Extended magnon states yield $r \approx 0$ for any size N whereas localized states develop a relationship of the form $R \equiv rN \propto N$.

Figure 2(a) shows R versus E for a representative value of the coupling disorder strength, $W_J = 0.5$. Calculations are done for system sizes of $N = 500$ up to $N = 2000$. We readily note that the magnon mode associated to $E = 0$ exhibits $R = 0$, which indicates a genuinely extended state. Indeed, in the absence of the external magnetic

field the zero-energy magnon mode is given by $|\psi_{\text{zero}}\rangle = (1/\sqrt{N})\sum_n |n\rangle$ despite the degree of the coupling disorder in W_J. Such an anomalous magnon mode with diverging localization length is supported by the correlation between matching diagonal and off-diagonal terms in the Heisenberg chain when $h_n = 0$ [cf. Eq. (4)] [34]. Conversely, localized modes are observed for $E > 0$, with R exhibiting a strong dependency on E. Figure 2(b) also shows r for a range of E and W_J.

The presence of a disordered magnetic field ($W_h \neq 0$) is expected to significantly impact the localization properties of the channel. We will see shortly that the magnon modes with energies in the immediate vicinity of $E = 0$ are particularly fragile in this respect.

3.2. Resonant state transfer mediated the uniform magnon mode

The extended magnon mode $|\psi_{\text{zero}}\rangle$ can mediate an almost perfect state transfer in the regime $g \ll 1$ given $h_0 = 0$, that is when the end spins are in exact resonance with that mode. In turn, the effective three-site Hamiltonian is spanned [41]:

$$\mathcal{H}^{(3)} = \begin{pmatrix} 0 & g\langle 2|\psi_{\text{zero}}\rangle & 0 \\ g\langle 2|\psi_{\text{zero}}\rangle & 0 & g\langle N+1|\psi_{\text{zero}}\rangle \\ 0 & g\langle N+1|\psi_{\text{zero}}\rangle & 0 \end{pmatrix}, \tag{7}$$

on the basis $\{|1\rangle, |\psi_{\text{zero}}\rangle, |N\rangle\}$. It is straightforward to show that the transfer time in this case is $\tau = \pi\sqrt{N}/\sqrt{2}g$.

It should be highlighted here that any other discrete mode $|\psi_k\rangle$ would provide us with an effective three-level as well given $h_0 = E_k$ [40]. If it allows for high-fidelity state transfer or not depends on symmetry between both effective couplings (typically destroyed by the disorder). Curiously, when N is even and also $W_J = 0$, there is another uniform mode at $E_{k'} = 1$ ($|v_{k',n}| = 1/\sqrt{N}$ for all n). The difference is that it comes with a well defined phase relationship between its components. Solving the time-independent Schrödinger equation for $v_{k',n}$ [see Eq. (4)], we obtain the rule $v_{k',n-1} = -v_{k',n+1}$, with $v_{k',2} = -v_{k',3}$ and $v_{k',N} = -v_{k',N+1}$. A quick inspection shows that these conditions cannot be fulfilled when N is odd. Furthermore, $|\psi_{k'}\rangle$ is unstable for any W_J and W_h. The uniqueness of the zero-energy mode $|\psi_{\text{zero}}\rangle$ lies in its perfect robustness against the coupling disorder W_J.

For the effective description in Eq. (7) to hold, interaction with the other modes $|\psi_k\rangle$ with $E_k \neq 0$ must be minimized. We expect that larger sizes N will demand smaller values of g as more modes appear in the vicinity of $E = 0$. Figure 3(a) shows the fidelity $F(\tau)$ evaluated over this parameter space for $W_J = 0.5$ in the absence of a magnetic field ($W_h = 0$). The contour lines cover points of constant $F(\tau)$. The logarithm scale enables us to identify a linear relationship between $\log N$ and $\log g$, which can generally be cast in the form $N^\mu \propto g^{-\nu}$. It is thus reasonable to assume that the fidelity scales as $F(\tau) = 1 - O(g^\nu N^\mu)$. Further numerical analysis in Figure 3(a) yields $\nu = 2$ and $\mu = 3$ to great accuracy. In fact, these exponents hold for the range of coupling disorder

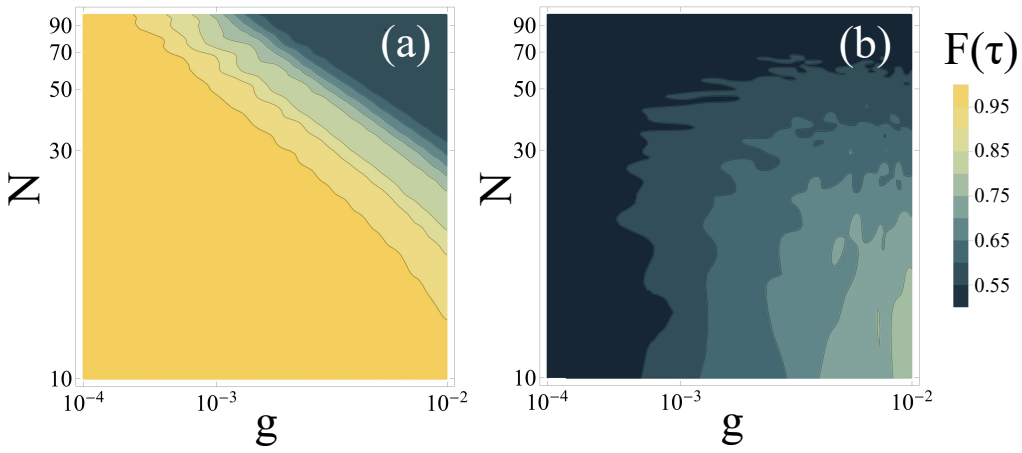

Figure 3. Contour plots (in log-log scale) of $F(\tau)$ in the (N, g) parameter space for (a) $W_h = 0$ and (b) $W_h = 0.05$, with $W_J = 0.5$ and $h_0 = 0$ in both cases. Data is obtained via exact diagonalization of 100 distinct realizations of the full Hamiltonian $\mathcal{H}$. Straight lines in (a) are associated to constant values of $F(\tau)$ and $g^\nu N^\mu$. A more detailed numerical analysis provides $\nu = 2$ and $\mu = 3$, such that the fidelity obeys the scaling law $F = 1 - O(g^2 N^3)$. Other values of $W_J < 1$ (weak disorder regime) in the absence of a magnetic field render similar plots. In (b) we emphasize how seriously the zero-energy uniform mode is affeceted by the presence of a disordered magnetic field given by $W_h = 0.05$.

considered in this work, $W_J < 1$. A high-fidelity state transfer is then guaranteed as long as $g \ll N^{-3/2}$. Setting $g = \epsilon N^{-3/2}$ close-to-perfect fidelities $F = 1 - O(\epsilon^2)$ can be achieved in a time $\tau \propto N^2/\epsilon$. We remark that it differs from the scaling of the transmission time in homogeneous isotropic XY chains with an odd number of sites, which is $\propto N/\epsilon$ [40].

Now, Fig. 3(b) shows what happens when we add a weakly disordered magnetic field ($W_h = 0.05$). Already at this level, the state transfer becomes quite ineffective. This occurs because, as pointed out earlier, the zero-energy mode $|\psi_{\text{zero}}\rangle$ cannot hold against the loss of correlation between diagonal and off-diagonal terms of the channel Hamiltonian. Add to this the fact that the all energy levels E_k of the channel fluctuates, no longer rendering a resonant interaction such as the one described in Eq. (7) at a *fixed* tuning energy h_0. Finally, we remark that the relatively good fidelities $F \approx 0.8$ seen in the bottom right corner Fig. 3(b) occur as a result of the small N and (not so small) $g \approx 0.01$ considered. In this particular scenario, the increasing of g invites the magnon modes closer to $E = 0$ to participate in the dynamics. At the stage set by $W_J = 0.5$ and $W_h = 0.05$, these modes are not seriously affected by the disorder. But then again, this is just a small-size effect that rapidly fades with N [cf. Fig. 2(a)].

3.3. Off-resonant state transfer

The situation described just above involving a disordered magnetic field, $W_h \neq 0$, and $N \gg 1$ can be resolved by setting an off-resonant state transfer protocol [40, 41, 42]. In

the regime $g \ll 1$, when $h_0 \neq E_k$ for all k, both end states $|1\rangle$ and $|N+2\rangle$ effectively behave as a two-level system described by the Hamiltonian [41]:

$$\mathcal{H}^{(2)} = \begin{pmatrix} \omega_1 & J_{\text{eff}} \\ J_{\text{eff}} & \omega_2 \end{pmatrix}, \tag{8}$$

where

$$\omega_1 = h_0 - g^2 \sum_k \frac{|v_{k,2}|^2}{E_k - h_0}, \tag{9}$$

$$\omega_2 = h_0 - g^2 \sum_k \frac{|v_{k,N-1}|^2}{E_k - h_0}, \tag{10}$$

$$J_{\text{eff}} = -g^2 \sum_k \frac{v_{k,2} v^*_{k,N-1}}{E_k - h_0}, \tag{11}$$

with the summations covering all $N-2$ modes of the channel.

In this interaction framework, end-to-end Rabi oscillations (two-level dynamics) are responsible for the state transfer. After diagonalization of the effective Hamiltonian above, it is straightforward to obtain the corresponding transition amplitude

$$a_N(t) = \frac{1}{\sqrt{\Delta^2_{\text{eff}}/4 + 1}} \sin\left[\left(\sqrt{\Delta^2_{\text{eff}}/4 + 1}\right) J_{\text{eff}} t\right], \tag{12}$$

where $\Delta_{\text{eff}} = (\omega_1 - \omega_2)/J_{\text{eff}}$ is effective detuning between the two renormalized diagonal energies. Given $\Delta_{\text{eff}} = 0$, which is ideal, the state transfer occurs at time $\tau = \pi/2|J_{\text{eff}}|$. This scenario is trivially met when the Hamiltonian of the channel possesses mirror symmetry or bipartite symmetry [31]. The first condition leads to $\omega_1 = \omega_2$ and the second one renders both summations in ω_1 and ω_2 null given h_0 is set right at the middle of the energy band. Note that quantum noise in general would be harmful to the protocol. Any dissipation rate should be small enough so that at least one half-cycle of the Rabi dynamics is completed. In adittion, based on the results obtained in [40] for the homogeneous channel (see [31] for arbitrary 1D channels), the transfer time scales as $\tau \sim 1/g^2$, with $F = 1 - O(g^2 N)$. Hence $g \ll \sqrt{N}$ to guarantee high fidelities.

Obviously, a fully disordered spin channel has neither of those two symmetries above. Nonetheless, it is possible to minimize Δ_{eff} by searching for magnon modes with some degree of symmetry left (say, by being nearly mirror symmetric with respect to the boundaries of the channel). This happens frequently, for instance, in channels featuring correlated disorder, where extended states are spanned among localized states (see, e.g., Refs. [43, 44]). For the sake of reference, a good fidelity must be larger than 2/3, which is the limit that can be achieved purely by classical means [22, 49]. This threshold corresponds to $\Delta_{\text{eff}} = 4.39$ [cf. Eqs. (3) and (12)]. Hence, effective detunings below this level must be sought.

While magnon modes with larger localization lengths are readily accessible in the vicinity of $E = 0$, at least for $W_h \ll 1$, let us look further into the spectrum for a more

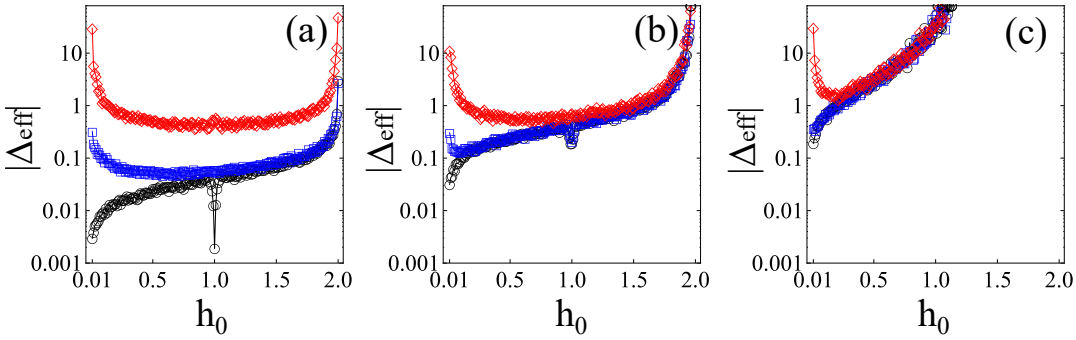

Figure 4. Absolute value of the effective detuning $\Delta_{\text{eff}} = (\omega_1 - \omega_2)/J_{\text{eff}}$ (in log scale), associated to Eq. (8), versus the tuning energy h_0. Data is obtained from exact numerical diagonalization of the channel Hamiltonian considering $N = 40$ for (a) $W_J = 0.01$, (b) $W_J = 0.1$, and (c) $W_J = 0.5$. The disorder strengths corresponding to the external magnetic field are $W_h = 0$ (black circles), $W_h = 0.01$ (blue squares), $W_h = 0.1$ (red diamonds). Displayed results are averaged over 100 independent disordered samples.

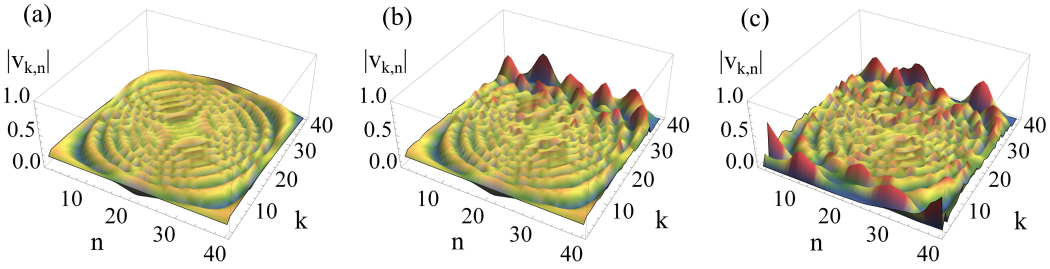

Figure 5. Spatial configuration of the channel modes given by $|v_{k,n}| = |\langle n|\psi_k\rangle|$ for $N = 40$ and disorder strengths $(W_J, W_h) = (0, 0), (0.1, 0)$, and $(0.1, 0.1)$ corresponding to panels (a), (b), and (c), respectively. Single typical realizations of the cases involving disorder are shown in (b,c). The mode index k is ordered with respect to increasing eigenvalues E_k.

comprehensive analysis. Figure 4 depicts Δ_{eff} over a range of tuning energies h_0 and various combinations of W_J and W_h. As suspected, having $h_0 \to 0$ is not a viable option when $W_h \neq 0$. Note that the coordinate $h_0 = 0$ is not included in the plots because the effective parameters [Eqs. (9) through (11)] diverge for $W_h = 0$. The role of each source of the disorder (diagonal and off-diagonal) is made evident in the figure. As W_J drives an asymmetric $\Delta_{\text{eff}} \times h_0$ profile – preserving extended states closer to zero-energy mode – the increase of W_h promotes strongly localized states at both boundaries of the energy band, a typical trait of Anderson localization. We also draw attention to the atypical drop in Δ_{eff} in the vicinity of $h_0 = 1$ for weak disorder [see Figs. 4(a) and 4(b)]. This is nothing but a residual response to the hitherto uniform mode k'. As explained earlier, this magnon mode is susceptible to both forms of disorder. Interestingly, the quantity Δ_{eff} also serves as a localization measure for the modes in the vicinity of h_0.

We get a better perspective of the localization landscape amid the influence of W_J and W_h in Fig. 5, where the spatial components of the magnon modes are shown

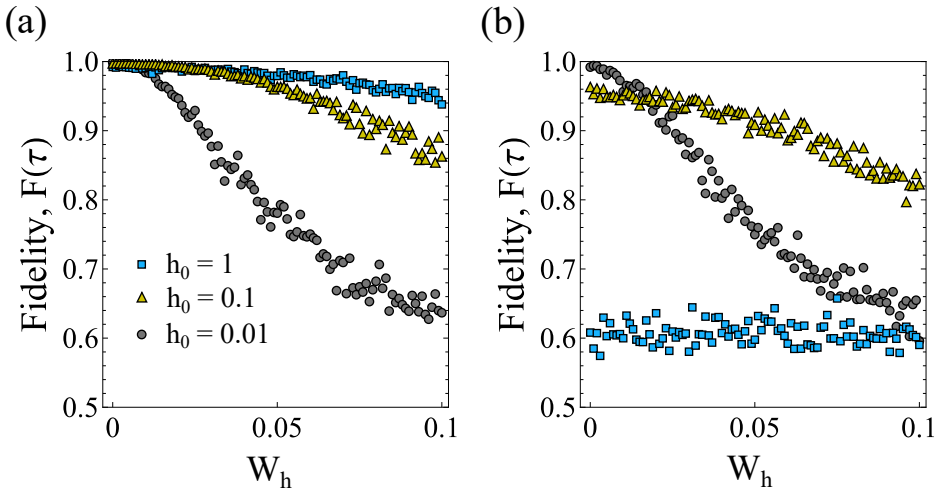

Figure 6. Transfer fidelity $F(\tau)$ versus magnetic-field disorder strength W_h for $N = 42$, $g = 10^{-4}$, (a) $W_J = 0.1$, and (b) $W_J = 0.5$. The tuning energies h_0 considered are specified on panel (a) and also applies to (b). Results are averaged over 100 independent realizations of the full Hamiltonian. The transfer time $\pi/2|J_{\text{eff}}|$ was set individually in each realization.

for selected parameters. In the clean case [Fig. 5(a)] extended modes fill the whole energy spectrum. Under the influence of the coupling disorder ($W_J = 0.1$) [Fig. 5(b)] localized states emerge as we depart from $E = 0$ (k is ordered with increasing E_k). Indeed, strongly localized modes are prominent at higher k values. It is also noteworthy that the low-energy region remains almost unaffected. Now, when the two forms of the disorder are acting upon the channel ($W_J = W_h = 0.1$) [Fig. 5(c)] both low- and high-energy spectrum boundaries are compromised. The spatial profile seen in Fig. 5(c) corresponds to the behavior of Δ_{eff} depicted by the red triangles in Fig. 4(b), where the middle of the energy band still offers conditions for high-fidelity state transfer.

The optimal value for h_0 hinges on the competition between W_J and W_h. Examining the data in Fig. 4, we realize that h_0 should generally be set around the center of the band against W_h, for low values of W_J. Indeed, by finally reporting on the fidelity outcomes $F(\tau) = F(\pi/2|J_{\text{eff}}|)$ for $W_J = 0.1$ in Fig. 6(a), we see that $h_0 = 1$ provides better resilience against W_h, followed by $h_0 = 0.1$, and $h_0 = 0.01$. The exception to that rule comes as W_J is high to such an extent that the only way to avoid $\Delta_{\text{eff}} > 4.39$ is by tuning h_0 to a level slightly above (but not so close to) zero [see, e.g., 4(c)]. Figure 6(b) confirms this behavior, where $h_0 = 0.1$ under entails the best state-transfer performance under $W_J = 0.5$, rendering fidelities above the classical threshold of 2/3 up to $W_h = 0.1$. Comparing Figs. 6(a) and 6(b), it is remarkable to observe how distinct the performances associated to $h_0 = 1$ are, what confirms that the middle of the band (and surroundings) should be avoided for higher values of the exchange coupling disorder W_h.

4. Conclusions

Spin waves offer novel pathways for signal processing, wave-based computation, and integration to quantum information processing devices [3]. By taking leverage of their high-degree of coherence, information can be encoded in the spin state and sent through relatively long channels even under considerable disorder.

We have seen that the landscape of localized states across the channel is defined by the interplay between the diagonal and off-diagonal disorder in the Heisenberg Hamiltonian. By properly navigating through the fluctuations via the tuning energy h_0, we showed that high-fidelity state transfer can be attained in different situations. In the scenario where only the $W_J \neq 0$, we may use the anomalous magnon mode at $E = h_0 = 0$ to mediate the state transfer between the ends of the chain. This mode is disorder-proof and yields a fidelity that scales as $F = 1 - O(\epsilon^2)$ occurring in a time $\tau \propto N^2/\epsilon$ given $\epsilon \ll 1$ (meaning $g \ll 1$). When both $W_J \neq 0$ and $W_h \neq 0$, then the Rabi-like (off-resonant, two-level) spin dynamics takes place. Depending on the value of W_J – which promotes an asymmetric distribution of the localization lengths throughout the spectrum – h_0 may be set not so far above $E = 0$, where the typical mode localization length is larger. Otherwise, when the influence of the diagonal disorder is more relevant, better state transfer performances are obtained by tuning h_0 to the middle of the band.

The ability to apply magnetic fields to individual spins without affecting neighboring spins poses a significant experimental challenge. However, recent advancements in atomic-scale magnetic field engineering provide encouraging evidence that selective magnetic field control is feasible at the level of individual spins, particularly in controlled low-temperature environments. For instance, a recent work [50] on single-atom magnets using dysprosium adsorbed on magnesium oxide surfaces demonstrated how dysprosium atoms can retain magnetic stability due to their high magnetic anisotropy energy. In these setups, the spins remain stable for extended periods, thus suggesting a route for local magnetic field tuning. This stability allows for targeted control of magnetic fields in atomic-scale systems, though these applications have thus far been successful primarily under ultra-low temperature conditions. While the disordered model described here requires experimental validation for systems containing tens of spins, our findings will inspire further developments in scalable spin systems designed for quantum state transfer. Note that the addressed protocol could be simulated in any platform able to perform tight-binding models, such as coupled waveguide arrays, where state-of-the-art technology allows for tuning of the parameters (diagonal and off-diagonal terms) with a high degree of control as done in, e.g., [48, 51, 52, 53] in various contexts. In such photonic settings, the exchange couplings would be defined by distance between adjacent waveguides and the effective potential would be given by the refractive index [53]. It is worth mentioning that the an experimental simulation of a perfect quantum state transfer protocol conceptualized for spin chains was performed in a waveguide array via judicious tuning of the coupling strengths [54]. In addition, there has been significant progress in realizations of quantum

information protocols in bulk materials [14, 55] (see also theoretical simulations in [56]) and quantum dots [57] mediated by exchange interactions.

Considering a realistic spin chain setting, the protocol implicitly demands very low temperatures. It is be possible to consider the effects of a heat bath using, for example, the Langevin formalism. In general terms, a Langevin bath would promote atomic vibrations, allowing, for instance, the alteration of spin-spin coupling. The resulting effective term would thus manifest as a time-dependent additional disorder distribution. We can then anticipate that high temperatures compromises the fidelity of the quantum state transfer protocol. Recall that the fidelity must be larger than the classical threshold of 2/3 so as to justify the use of a quantum channel. Nevertheless, proper encoding schemes and choice of the spin network topology can be used to mitigate temperature effects [58, 59, 60]. These, on the other hand, may be less detrimental to long-range interacting spins [61]. Considering, e.g., cold atoms in optical tweezers [62] as a promising platform to realize spin models, finite temperature can cause positional disorder in the particles [61].

Here, we did not attempt to derive general scaling laws for the fidelity or the optimal h_0 with respect to the disorder parameters W_J and W_h. This can be done in future works. Rather, we wanted to focus on the use of the anomalous magnon mode and the nearby extended states as a mean to achieve high-fidelity state transfer despite the disorder. Amid the fast and remarkable progress in the field of magnonics, including its integration with quantum information processing concepts [10], we hope to see more research addressing the role of disorder in magnon-based quantum communication.

Acknowledgments

This work was supported by CNPq, CAPES, FINEP (Federal Brazilian Agencies), FAPEAL (Alagoas State Agency), and FACEPE (Pernambuco State Agency).

References

[1] Hoffmann A and Bader S D 2015 *Phys. Rev. Appl.* **4**(4) 047001
[2] Vedmedenko E Y, Kawakami R K, Sheka D D, Gambardella P, Kirilyuk A, Hirohata A, Binek C, Chubykalo-Fesenko O, Sanvito S, Kirby B J, Grollier J, Everschor-Sitte K, Kampfrath T, You C Y and Berger A 2020 *Journal of Physics D: Applied Physics* **53** 453001
[3] Pirro P, Vasyuchka V I, Serga A A and Hillebrands B 2021 *Nature Reviews Materials* **6** 1114–1135
[4] Chumak A V, Serga A A and Hillebrands B 2014 *Nature Communications* **5** 4700
[5] Elyasi M, Sato K and Bauer G E W 2019 *Phys. Rev. B* **99**(13) 134402
[6] Mohseni M, Qaiumzadeh A, Serga A A, Brataas A, Hillebrands B and Pirro P 2020 *New Journal of Physics* **22** 083080
[7] Divinskiy B, Merbouche H, Demidov V E, Nikolaev K O, Soumah L, Gouéré D, Lebrun R, Cros V, Youssef J B, Bortolotti P, Anane A and Demokritov S O 2021 *Nature Communications* **12** 6541
[8] Csaba G, Ádám Papp and Porod W 2017 *Physics Letters A* **381** 1471–1476
[9] Han J, Cheng R, Liu L, Ohno H and Fukami S 2023 *Nature Materials* **22** 684–695

[10] Yuan H, Cao Y, Kamra A, Duine R A and Yan P 2022 *Physics Reports* **965** 1–74 quantum magnonics: When magnon spintronics meets quantum information science
[11] Lachance-Quirion D, Tabuchi Y, Gloppe A, Usami K and Nakamura Y 2019 *Applied Physics Express* **12** 070101
[12] Fukuhara T, Kantian A, Endres M, Cheneau M, Schausz P, Hild S, Bellem D, Schollwock U, Giamarchi T, Gross C, Bloch I and Kuhr S 2013 *Nat Phys* **9** 235–241
[13] Fukuhara T, Hild S, Zeiher J, Schauß P, Bloch I, Endres M and Gross C 2015 *Phys. Rev. Lett.* **115**(3) 035302
[14] Sahling S, Remenyi G, Paulsen C, Monceau P, Saligrama V, Marin C, Revcolevschi A, Regnault L P, Raymond S and Lorenzo J E 2015 *Nature Physics* **11** 255–260
[15] Cornelissen L J, Liu J, Duine R A, Youssef J B and van Wees B J 2015 *Nature Physics* **11** 1022–1026
[16] Liu C, Chen J, Liu T, Heimbach F, Yu H, Xiao Y, Hu J, Liu M, Chang H, Stueckler T, Tu S, Zhang Y, Zhang Y, Gao P, Liao Z, Yu D, Xia K, Lei N, Zhao W and Wu M 2018 *Nature Communications* **9** 738
[17] Mathew G, Silva S L L, Jain A, Mohan A, Adroja D T, Sakai V G, Tomy C V, Banerjee A, Goreti R, N A V, Singh R and Jaiswal-Nagar D 2020 *Phys. Rev. Res.* **2**(4) 043329
[18] Li J, Wang Y P, Wu W J, Zhu S Y and You J 2021 *PRX Quantum* **2**(4) 040344
[19] Kiely A and Campbell S 2021 *New Journal of Physics* **23** 033033
[20] Yan Y T, Zhao C, Yang Z, Wang D W and Zhou L 2022 *Journal of Physics B: Atomic, Molecular and Optical Physics* **55** 195502
[21] Bao X X, Guo G F, Yang X and Tan L 2023 *Chinese Physics B* **32** 080301
[22] Bose S 2003 *Phys. Rev. Lett.* **91**(20) 207901
[23] Christandl M, Datta N, Ekert A and Landahl A J 2004 *Phys. Rev. Lett.* **92**(18) 187902
[24] Plenio M B, Hartley J and Eisert J 2004 *New Journal of Physics* **6** 36
[25] Banchi L, Apollaro T J G, Cuccoli A, Vaia R and Verrucchi P 2010 *Phys. Rev. A* **82**(5) 052321
[26] Apollaro T J G, Banchi L, Cuccoli A, Vaia R and Verrucchi P 2012 *Phys. Rev. A* **85**(5) 052319
[27] Lorenzo S, Apollaro T J G, Sindona A and Plastina F 2013 *Phys. Rev. A* **87**(4) 042313
[28] Gualdi G, Kostak V, Marzoli I and Tombesi P 2008 *Phys. Rev. A* **78**(2) 022325
[29] Almeida G M A, Ciccarello F, Apollaro T J G and Souza A M C 2016 *Phys. Rev. A* **93**(3) 032310
[30] Estarellas M P, D'Amico I and Spiller T P 2017 *Phys. Rev. A* **95**(4) 042335
[31] Almeida G M A 2018 *Phys. Rev. A* **98**(1) 012334
[32] Apollaro T J G, Almeida G M A, Lorenzo S, Ferraro A and Paganelli S 2019 *Phys. Rev. A* **100**(5) 052308
[33] Almeida G M A, Dutra R F, Souza A M C, Lyra M L and de Moura F A B F 2023 *Phys. Rev. A* **108**(2) 022407
[34] de Moura F A B F, Coutinho-Filho M D, Raposo E P and Lyra M L 2002 *Phys. Rev. B* **66**(1) 014418
[35] De Chiara G, Rossini D, Montangero S and Fazio R 2005 *Phys. Rev. A* **72**(1) 012323
[36] Giampaolo S M and Illuminati F 2010 *New Journal of Physics* **12** 025019
[37] Zwick A, Álvarez G A, Stolze J and Osenda O 2012 *Phys. Rev. A* **85**(1) 012318
[38] Zwick A, Álvarez G A, Stolze J and Osenda O 2015 *Quant. Inf. Comp.* **15** 852
[39] Kay A 2016 *Phys. Rev. A* **93**(4) 042320
[40] Wójcik A, Łuczak T, Kurzyński P, Grudka A, Gdala T and Bednarska M 2005 *Phys. Rev. A* **72**(3) 034303
[41] Wójcik A, Łuczak T, Kurzyński P, Grudka A, Gdala T and Bednarska M 2007 *Phys. Rev. A* **75**(2) 022330
[42] Almeida G M A, de Moura F A B F and Lyra M L 2018 *Phys. Lett. A* **382** 1335
[43] Almeida G M A, de Moura F A B F and Lyra M L 2019 *Quantum Information Processing* **18** 41
[44] Almeida G M A, de Moura F A B F and Lyra M L 2019 *Quant. Inf. Proc.* **18** 350
[45] Júnior P, Almeida G, Lyra M and de Moura F 2019 *Physics Letters A* **383** 1845–1849

[46] Junior M, de Lima W, Teixeira V, da Fonseca D, Moraes F, Barbosa A, Almeida G and de Moura F 2023 *Journal of Magnetism and Magnetic Materials* **579** 170880
[47] Izrailev F, Krokhin A and Makarov N 2012 *Physics Reports* **512** 125 – 254
[48] Pitsios I, Banchi L, Rab A S, Bentivegna M, Caprara D, Crespi A, Spagnolo N, Bose S, Mataloni P, Osellame R and Sciarrino F 2017 *Nature Communications* **8** 1569
[49] Horodecki M, Horodecki P and Horodecki R 1999 *Phys. Rev. A* **60**(3) 1888–1898
[50] Singha A, Willke P, Bilgeri T, Zhang X, Brune H, Donati F, Heinrich A J and Choi T 2021 *Nature Communications* **12** 4179
[51] Rivas D, Szameit A and Vicencio R A 2020 *Scientific Reports* **10** 13064
[52] Xu Z S, Gao J, Krishna G, Steinhauer S, Zwiller V and Elshaari A W 2022 *Photon. Res.* **10** 2901–2907
[53] Gao J, Xu Z S, Yang Z, Zwiller V and Elshaari A W 2024 *npj Nanophotonics* **1** 34
[54] Chapman R J, Santandrea M, Huang Z, Corrielli G, Crespi A, Yung M H, Osellame R and Peruzzo A 2016 *Nat. Comm.* **7** 11339
[55] Choi D J, Robles R, Yan S, Burgess J A J, Rolf-Pissarczyk S, Gauyacq J P, Lorente N, Ternes M and Loth S 2017 *Nano Letters* **17** 6203–6209
[56] Bazhanov D I, Sivkov I N and Stepanyuk V S 2018 *Scientific Reports* **8** 14118
[57] Kandel Y P, Qiao H, Fallahi S, Gardner G C, Manfra M J and Nichol J M 2019 *Nature* **573** 553–557
[58] Cappellaro P, Viola L and Ramanathan C 2011 *Phys. Rev. A* **83**(3) 032304
[59] Ajoy A and Cappellaro P 2012 *Phys. Rev. A* **85**(4) 042305
[60] Banchi L 2013 *The European Physical Journal Plus* **128** 137
[61] Hermes S, Apollaro T J G, Paganelli S and Macrì T 2020 *Phys. Rev. A* **101**(5) 053607
[62] Kaufman A M and Ni K K 2021 *Nature Physics* **17** 1324–1333